A multi-objective optimization strategy for ultra-low energy residential buildings based on a hybrid machine learning algorithm

Yanzhe Yu[1,2], Xingxin Chen[1], Xingguo Guo[1,2,*], Wenhua Chen[1,2], Shen Wei[3]

1 = ***School of Infrastructure Engineering, Nanchang University, Nanchang, China***

2 = ***Jiangxi Province Key Laboratory of Advanced Civil Engineering Materials and Green Intelligent Construction, Nanchang, 330031, China***

3 = ***The Bartlett School of Sustainable Construction, University College London (UCL), 1-19 Torrington Place, London, WC1E 7HB, United Kingdom***

* Corresponding author. Email address: guoxingguo@ncu.edu.cn (X. Guo).

Email addresses:

yanzhe_yu@ncu.edu.cn (Y. Yu), 412500220038@email.ncu.edu.cn (X. Chen), guoxingguo@ncu.edu.cn (X. Guo), chenwenhua14@tju.edu.cn (W. Chen) and shen.wei@ucl.ac.uk (S. Wei).

Nomenclature

Nomenclature			
Abbreviation			
ANN	Artificial Neural Network	LCC	Life Cycle Cost
BEC	Building Energy Consumption	MAPE	Mean Absolute Percentage Error
CNY	Chinese Yuan	MOO	Multi-Objective Optimization
COP	Coefficient of Performance	MOPSO	Multi-Objective Particle Swarm Optimization
EUI	Energy Use Intensity	MSE	Mean Squared Error
EPS	Expanded Polystyrene	NSGA	Non-dominated Sorting Genetic Algorithm
GBDT	Gradient Boosting Decision Tree	PMV	Predicted Mean Vote
HSCW	Hot Summer and Cold Winter	PPD	Predicted Percentage of Dissatisfaction
HSWW	Hot Summer and Warm Winter	SHGC	Solar Heat Gain Coefficient
HV	Hypervolume	ULEBs	Ultra-Low Energy Buildings
IGD	Inverted Generational Distance	WWR	Window-to-Wall Ratio
ITC	Indoor Thermal Comfort	XPS	Extruded Polystyrene

Abstract

To address the lack of effective multi-objective optimization approaches that balance building energy consumption, indoor thermal comfort, and life-cycle cost in ultra-low energy residential buildings, this study proposes a hybrid algorithm that integrates the Non-dominated Sorting Genetic Algorithm-II (NSGA-II) with Multi-Objective Particle Swarm Optimization (MOPSO) for the multi-objective optimization design of such buildings, validated through case studies in two climate zones. Orthogonal experiments were conducted on eight variables, including the heat transfer coefficients of external walls, roofs, and windows; directional window-to-wall ratios; and solar heat gain coefficients. An artificial neural network model for the three objectives was developed to serve as fitness functions for the hybrid algorithm. The hybrid approach outperformed the standalone NSGA-II and MOPSO in terms of the hypervolume, inverted generational distance, and spacing metrics, demonstrating superior convergence and solution diversity. Optimized design parameter ranges were derived, and best solutions were identified for both climates, providing practical guidance for similar regions. The innovations of this study include: (1) a multi-objective optimization framework balancing energy, comfort, and cost to enhance solution practicality in ultra-low energy residential buildings; (2) integration of NSGA-II-MOPSO with metamodeling for the three objectives, verified to improve optimization efficiency over individual algorithms.

Keywords: Building performance, multi-objective optimization, ultra-low energy residential buildings, NSGA-II-MOPSO, Climate-responsive design

1. Introduction

Building operations account for approximately 30% of the global final energy consumption, with residential buildings contributing 70% [1,2]. Urbanization and climate change have further increased energy demand in urban residential sectors, which now represent a quarter of the global final energy use (excluding non-energy use) [3,4]. To advance building energy efficiency, concepts such as Ultra-Low Energy Buildings (ULEBs) have emerged as key strategies for achieving energy savings and decarbonization [5,6]. ULEBs, however, aim for not only low operational energy consumption, but also improved quality-of-life demands and reduced cost from other construction-related activities [7]. Building Energy Consumption (BEC), Indoor Thermal Comfort (ITC), and Life Cycle Cost (LCC) are commonly used as metrics for evaluating the overall performance of buildings [8,9]. These metrics, however, often conflict. For example, enhancing ITC usually requires higher energy consumption, resulting in higher LCC. Influenced by envelope components and climate, balancing these metrics in ULEBs remains challenging [10].

To address these conflicting metrics, scholars have proposed Multi-Objective Optimization (MOO) for residential building design [11–13]. For example, Wang et al. [14] optimized the BEC and ITC in cold-region passive buildings using a Non-dominated Sorting Genetic Algorithm-II (NSGA-II), coupled with a redundancy analysis and Gradient Boosted Decision Tree (GBDT). In Greece, Kilis et al. [15] explored MOO approaches for optimizing building envelope thermal design and demonstrated that contradictions between optimization criteria in single-objective optimization underscored the necessity of balancing these criteria using MOO. Xue et al. [16] constructed a building energy model with hybrid ventilation and light-dimming control in EnergyPlus, and developed an NSGA-II algorithm to find optimal design solutions that minimize the LCC and emissions. Gou et al. [17] conducted MOO using NSGA-II coupled with an Artificial Neural Network (ANN). Their work showed significant potential for enhancing ITC with a lower BEC for residential buildings in Shanghai. Existing studies have employed diverse methods: MOO models based on the

harmony search algorithm [18], simulation modeling with sensitivity analysis [19], integration of NSGA-II with EnergyPlus [20], and performance-responsive generative frameworks combining multi-agent systems, genetic algorithms, and ANN [21].

Current MOO relies on two approaches: coupling simulation tools with optimization algorithms (often time-consuming, limiting practical use) or using metamodels (surrogate models) to reduce computational time [22–24]. While metamodels are widely adopted, balancing efficiency and robustness remains a focus [10,25]. To improve predictive accuracy, Chen et al. [26] improved the accuracy of a backpropagation neural network for predicting carbon emissions, discomfort hours, and costs via a random grid search. However, this method is computationally intensive, which hinders its efficiency. Against the need to optimize public education buildings for daylighting and thermal comfort, Xu et al. [27] proposed a two-stage meta-model MOO method, where an ANN was coupled separately with NSGA-II and MOPSO to optimize building envelopes. Validated via a typical teaching building case, the method compared the performances of NSGA-II and MOPSO and derived optimal envelope designs. Moreover, complex real-world MOO problems exceed the capacity of a single algorithm, which suffers from inherent limitations [28]. For example, NSGA-II, a widely used algorithm based on genetic algorithms, demonstrates a strong global search capability [29]. However, it suffers from relatively a slow convergence [30]. In contrast, the Multi-Objective Particle Swarm Optimization (MOPSO) algorithm, which is derived from the particle swarm optimization approach, offers a simple structure and fast convergence speed [31]. Nevertheless, it is more prone to being trapped in local optima [32]. Existing studies have developed hybrid algorithms to overcome single-algorithm limitations, such as in optimizing building envelopes integrated with power generation systems [33] and enhancing public building performance [34,35]. However, relevant studies on residential building performance MOO remain unreported.

Table 1: Summary of recent literature on residential building performance optimization.

Ref.	Year	Climate zone	Objectives	Optimization algorithms	Fitness function	Performance indicators of MOO algorithms	Statistical analysis
[36]	2020	Cold zone	LCC, GWP, CTR	NSGA-II	GBDT	-	LHS, PRCC
[14]	2020	Cold zone	EUI, CTR	NSGA-II	GBDT	-	LHS, PRCC
[37]	2020	Cold zone	EUI, PPD, SDA	SPEA-2	Coupling simulation with MOO algorithms	Hypervolume	-
[13]	2021	Cold and temperate zones	Overall Energy Need, IIC	NSGA-II	Coupling simulation with MOO algorithms	-	-
[19]	2021	South Korea	LCC, GWP, AED	NSGA– II	ANN	-	LHS, Sobol's method
[8]	2021	HSCW zone	EUI, DTR, LCC	NSGA– II	Coupling simulation with MOO algorithms	-	Influence coefficient
[29]	2021	Cfa climate	Energy for heating and cooling, DTR	NSGA– II	Coupling simulation with MOO algorithms	Hypervolume	LHS, standardized regression coefficient, p-value
[38]	2022	Cold, semi-arid zone	HLE, UDI, PTC	NSGA-III	PCA-ANN	Hypervolume	LHS
[16]	2022	Severe cold zone	LCC, LCCE	NSGA-II	ANN	-	SRRC, PRCC
[39]	2023	Cold zone	AED, SUH	NSGA-II	GA-RBF	-	NCA
[40]	2023	HSCW zone	Embodied and operational GWP	NSGA-II	LSSVM	-	-

[41]	2024	HSCW zone	EUI, PPD, UDI	NSGA-II	BO-XGBoost	-	". get_score" method
[21]	2025	Cold zone	UDI, PPD, indoor CO_2 concentration	NSGA-II	backpropagation neural network	Hypervolume	LHS, extended fourier amplitude sensitivity test
[42]	2025	Cold zone	AED, DTR, LCCE	NSGA-III	ANN	-	The Morris method
[43]	2025	HSCW zone	EUI, PMV, cost	NSGA-II	LSTM	Hypervolume	Pearson correlation
[44]	2025	Cold zone	EUI, DTR, IIC	NSGA-II	GA-BPNN	-	LHS
This study		HSCW and HSWW zones	BEC, ITC, LCC	NSGA-II-MOPSO	ANN	Hypervolume, IGD and Spacing	Mean squared error, mean absolute percentage error, PRCC

Notes: AED = annual energy demand; BO-XGBoost = Bayesian optimization with extreme gradient boosting trees; CTR= comfort time ratio; DTR = discomfort time ratio; EUI = energy use intensity; GWP = global warming potential; HLE = heating and lighting energy; HSWW = Hot Summer and Warm Winter; IIC = initial investment cost; IGD = inverted generational distance; LCCE = Life-cycle carbon emissions; LHS = Latin hypercube sampling; LSTM = long short-term memory; LSSVM = least squares support vector machine; NCA = neighborhood components analysis; PRCC = partial rank correlation coefficient; PRCC = partial rank correlation coefficient; PTC = percentage of thermal comfort; RBF = radial basis function; UDI= useful daylight illuminance; SDA = spatial daylight autonomy; SPEA = strength pareto evolutionary algorithm; SRRC = standard rank regression coefficient; SUH = summer discomfort hours.

Table 1 summarizes recent research on the MOO of residential building performance. As shown in the table, most studies employed NSGA-II as the optimization method; however, there is limited discussion regarding the performance and improvement of the optimization algorithms. To enhance the overall optimization performance, this study proposed a hybrid algorithm, NSGA-II-MOPSO, which combines the strengths of both algorithms. This hybrid approach retains the global search ability of NSGA-II and incorporates the fast convergence characteristics of MOPSO. First, eight design variables were selected, and an orthogonal experiment was conducted. Based on simulation data from the DesignBuilder software, an ANN model was established to predict the BEC, ITC, and LCC. The NSGA-II-MOPSO algorithm was developed for MOO and best solutions for the ultra-low energy building in selected case-study cities. The innovation of this study lies in (1) proposing an MOO framework for ultra-low energy buildings to balance BEC, ITC and LCC. This will make the optimization solutions more practical and provide a reference for future studies. (2) NSGA-II-MOPSO was integrated into metamodel development for BEC, ITC, and LCC, with verified efficiency against NSGA-II and MOPSO.

2. Methodology

2.1 Research design

This study proposed a three-objective optimization method for ultra-low energy residential buildings in the HSCW zone using the NSGA-II-MOPSO algorithm, aiming to improve the ITC, reduce the BEC, and lower the LCC by adjusting building design parameters during the design phase. First, eight key building design parameters were identified. An orthogonal experimental design was applied to generate 49 sample sets based on the defined parameter ranges. Subsequently, the ITC, BEC, and LCC of the residential building were simulated using DesignBuilder v6.1.0.6 to generate the datasets. Second, the datasets underwent preprocessing and were divided into a training set (80%) and a test set (20%) for ANN model development. The prediction accuracy of the model was evaluated using the coefficient of determination (R^2). Third, the trained ANN model was integrated as a fitness function into the MOO framework. The

NSGA-II-MOPSO model was constructed by incorporating the constraint ranges of the design parameters, resulting in the generation of a Pareto optimal solution set. To ensure fairness in algorithm comparisons, all calculations were performed under consistent computational conditions: the same computer, identical MATLAB version, and a runtime environment with only MATLAB active.

2.2 Case study

As the world's largest energy consumer, China prioritizes residential energy savings [45]. China's building operational energy use reached 1.06 billion tons of standard coal equivalent (tce), with residential buildings accounting for 61% of the total [41,46]. Notably, China's Hot Summer and Cold Winter (HSCW) zone, home to 600 million people and contributing nearly half of the national economy, has substantial residential energy-saving potential [47,48]. In China, ULEBs are viewed as a foundational step toward zero-energy buildings; however, their promotion is limited in southern regions compared to that in northern China. This disparity likely stems from the origins of the relevant standards and designs in high-latitude Western European regions, leaving a shortage of optimized design methods for ULEB in southern regions [7,8].

This study applied the proposed MOO methodology to a case building in Nanchang, with a comparative analysis conducted for Guangzhou. The case building is a slab-type apartment, a typical residential type in southern China. Outdoor meteorological parameters for both locations were obtained from typical meteorological year data, as illustrated in Figure 1. Nanchang, situated in the HSCW zone, experiences sweltering and humid summers alongside cold and damp winters. In contrast, Guangzhou is located in the HSWW zone, characterized by long, hot summers and mild winters with no significant cold period. According to JGJ/T 346-2014 *Standard for weather data of building energy efficiency*, the heating degree days (HDD_{18}) and cooling degree days (CDD_{26}) (units: °C·d) in Nanchang are 1326 and 250, respectively, while those in Guangzhou are 373 and 313. These distinct climatic conditions lead to different energy demands: a balanced requirement for both heating and cooling in Nanchang versus a

predominant cooling load in Guangzhou.

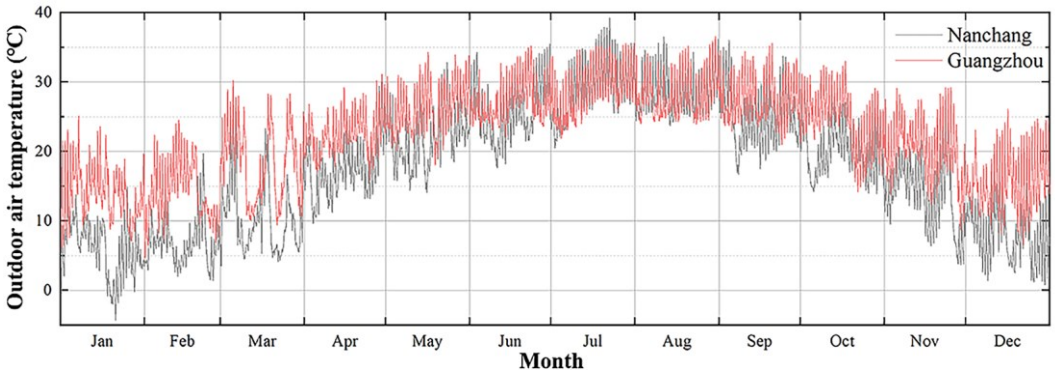

Figure 1. Outdoor air temperatures of two cities. (Data source: https://energyplus.net/weather)

The building was modeled using DesignBuilder, and a three-dimensional model is presented in Figure 2. It has a total floor area of 3145.65 m², five floors with a height of 3 m, and a north-south orientation. The envelope structure, including the external walls, roofs, interior walls, external windows, and floor slabs, is detailed in Table 2, with the key thermal parameters of the building materials listed in Table 3. Tables 2 and 3 present detailed thermal performance data of the case building envelope. These data are derived from the architectural drawings of the case building and serve as the initial parameter set for simulation calculations in the software, as well as a baseline for comparison following subsequent optimization. The external windows are aluminum alloy with a Solar Heat Gain Coefficient (SHGC) of 0.75, and the Window-to-Wall Ratios (WWRs) are east (0.02), south (0.40), west (0.02), and north (0.25).

Figure 2. Case-building model.

Table 2: Building envelope structure parameters.

Building envelope	Structure (from the outside to the inside)	U-value W/(m²·K)
External wall	Cement mortar (20mm) + EPS (30mm) + Shale sintered porous bricks (240mm) + cement mortar (20mm)	0.65
Roof	Cement mortar (20mm) + EPS (100mm) + waterproof roll (4mm) + cement mortar (20mm) + reinforced concrete (100mm)	0.62
Internal wall	Cement mortar (20mm) + Shale sintered porous bricks (240mm) + cement mortar (20mm)	1.58
Floor	Cement mortar (20mm) + reinforced concrete (100mm)	2.55
Door	Steel door (60mm)	2.55
External window	Aluminum alloy profile window frame + single-glass (6mm)	5.80

Table 3: Thermal parameters of building materials.

Materials	Thermal conductivity W/(m·K)	Density (kg/m^3)	Specific heat capacity J/(kg·K)
Cement mortar	0.93	1800	1050
EPS	0.046	19	2035
Porous bricks	0.73	780	1150
Waterproof roll	0.23	900	1620
Reinforced concrete	1.74	2500	935.2

The indoor environment, occupant activities, equipment lighting, etc., of the residential buildings all meet the relevant regulations in GB 55015-2021 *General code for energy efficiency and renewable energy application in buildings* [49] and GB/T 51350-2019 *Technical standard for nearly zero-energy buildings* [50]. According to the standards, the summer cooling set temperature of air-conditioned rooms was set to 26 ℃, the winter heating set temperature was set to 20 ℃, and the indoor per capita fresh air volume was 30 m³/(h·person). In addition, the Coefficient of Performance (COP) of the

air conditioning system was set to 3.5, according to GB 55015-2021.

Figure 3 shows the operating schedule of the ultra-low energy residential building. Figure 3(a) shows the occupancy rates of the personnel in each room. The schedules of each room were consistent with human daily life patterns, and the per capita floor area was 32 m². The number of personnel in the stairwell can be ignored. Figure 3(b) shows the schedule for the lighting usage rate in each room. According to GB 55015-2021, the lighting power densities of the bedroom, living room, kitchen, and bathroom were 4, 6, 6, and 4 W/m², respectively. Figure 3(c) shows the schedule of the equipment utilization rate for different room types. The equipment power densities of the bedroom, living room, kitchen, and bathroom were 6, 6, 24 W/m², and the equipment power respectively. Figure 3(d) shows the schedule of air conditioning operation in different rooms. For residential buildings, bedrooms and living rooms require heating and cooling, whereas other rooms adopt natural ventilation only. In addition, a 100% occupancy rate in the living room indicated that the air conditioner was in an open state and a 0% occupancy rate indicated that it was closed.

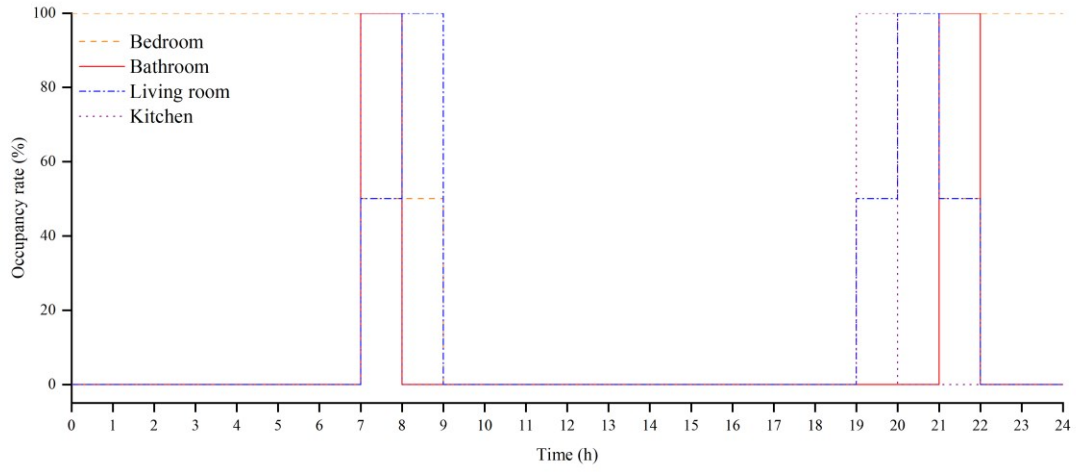

(a) Personnel occupancy rate

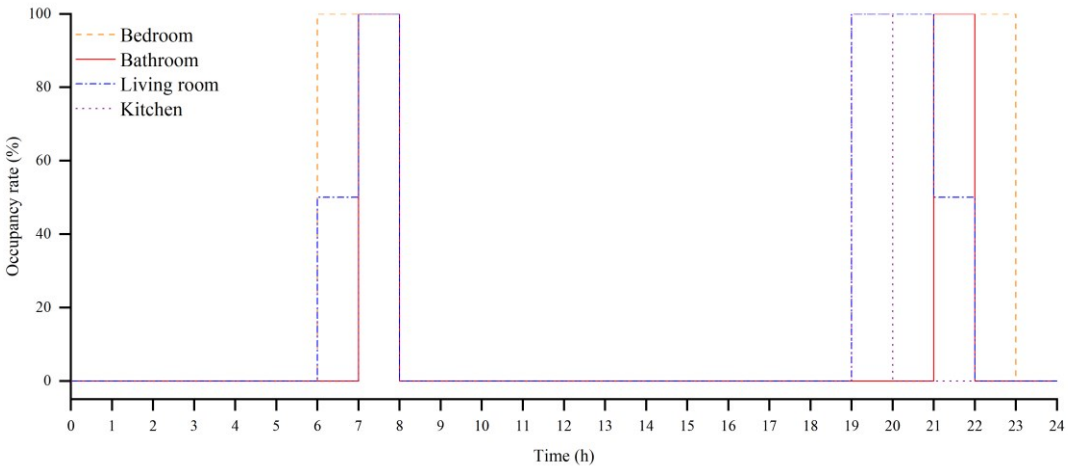

(b) Lighting occupancy rate

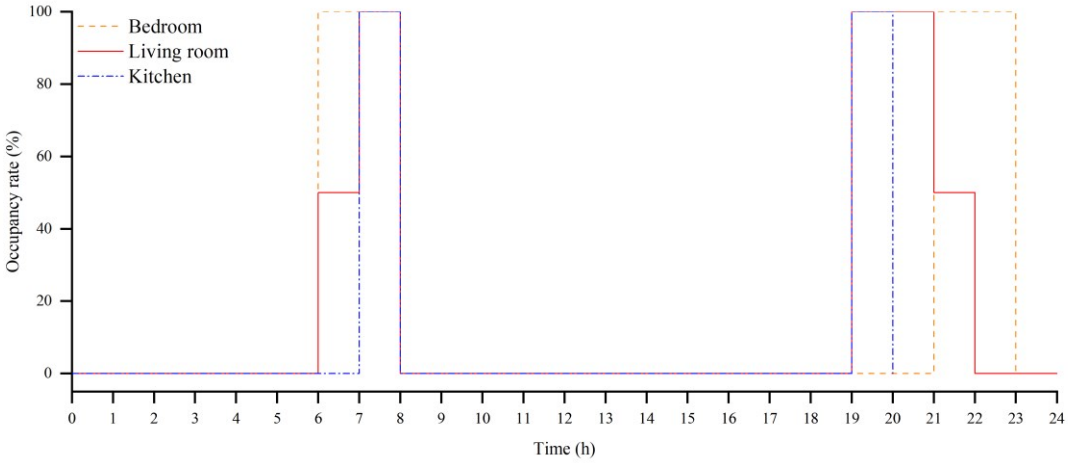

(c) Equipment occupancy rate

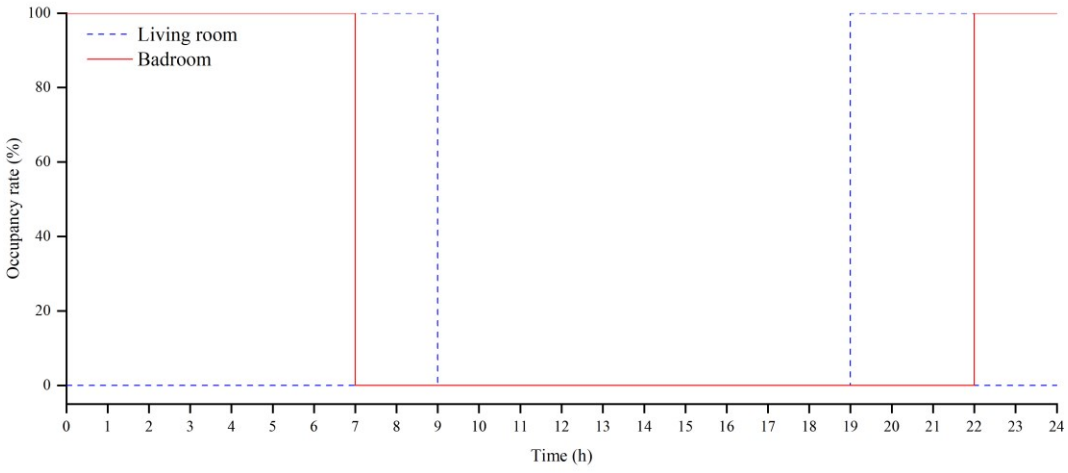

(d) HVAC system runtime

Figure 3. Building a runtime schedule.

Furthermore, to ensure the accuracy of the ITC simulation, this study set the clothing thermal resistance and human metabolic rate according to the different room types and seasons. The clothing thermal resistance for the bedroom was set at 2.8 clo in winter, 1.3 clo in summer, and 2.2 clo in transitional seasons; the human metabolic rate was set at 0.7 met [51]. For rooms other than the bedroom, the clothing thermal resistance was set at 1.5 clo in winter, 0.3 clo in summer, and 0.8 clo in transitional seasons; the human metabolic rate was 1 met [52].

2.3 Building performance simulation

2.3.1 Selection of design variables

To optimize ultra-low energy residential buildings considering the BEC, ITC, and LCC, design variables were selected based on their impact on the objectives and engineering practicality. The external wall and roof heat transfer coefficients (U-values) are key envelope parameters that reduce unwanted heat transfer, stabilize indoor temperatures, and balance LCC through insulation costs [53,54]. The WWR was considered separately for the north, south, east, and west orientations to adapt to directional solar radiation and daylight, balancing solar heat gain/loss and daylight availability, while affecting the LCC. The external window U-value addresses the thermal weakness of windows by reducing heat loss, improving thermal stability, and influencing the LCC via manufacturing costs. The SHGC controls solar heat entry, reducing cooling loads and improving ITC, with glazing costs impacting LCC. Orientation, shading, and natural ventilation were excluded: orientation is site-specific and indirectly captured by directional WWR; shading can be achieved through WWR and SHGC, avoiding added complexity; natural ventilation depends on variable weather and design factors, making it impractical for airtight envelopes and beyond this study's scope [29]. Thus, eight variables were included: the external wall and roof U-values, WWR per orientation, window U-value, and SHGC.

According to GB 55015-2021 [49] and GB/T 51350-2019 [50], ultra-low energy

residential buildings in the HSCW zone must have external wall and roof U-values not exceeding 0.40 W/(m²·K) and 0.35 W/(m²·K), respectively. The maximum WWR limits for the east, south, west, and north orientations were 0.35, 0.45, 0.35, and 0.40, respectively. Lower WWR limits for each orientation were calculated based on the requirement that the main rooms' window-to-floor area ratio should not be less than 1/7. The external window U-values and SHGC values must also comply with the design standards. To facilitate cost analysis and result application, both the thickness and U-value were employed for building envelope analysis. The optimized U-values were accordingly derived via conversion, based on the analysis of the variation range of insulation layer thickness within the Pareto optimal solution set. The same method for defining the design variable ranges in the HSCW zone was applied to the HSWW zone. Table 4 lists the optimization variables and their ranges for both zones.

Table 4: Design variables and range values of ultra-low energy residential buildings in the HSCW and HSWW zones.

Categories	Parameters	Unit	Range of values	
			HSCW	HSWW
Wall	U-value	W/(m²·K)	[0.15, 0.40]	[0.30, 0.80]
Roof	U-value	W/(m²·K)	[0.15, 0.35]	[0.25, 0.40]
WWR	East	-	[0.10, 0.35]	[0.10, 0.30]
	South	-	[0.20, 0.45]	[0.20, 0.40]
	West	-	[0.10, 0.35]	[0.10, 0.30]
	North	-	[0.15, 0.40]	[0.15, 0.40]
Window	U-value	W/(m²·K)	[1.00, 2.50]	[1.00, 2.50]
	SHGC	-	[0.10, 0.40]	[0.10, 0.30]

2.3.2 Calculation of the optimization objectives

In the optimization design of ultra-low energy residential buildings, besides reducing the BEC, it is also important to consider the balance between occupant comfort and economic performance. Therefore, this study used Energy Use Intensity (EUI), ITC, and LCC as optimization objectives.

(1) Annual EUI: The annual EUI refers to the energy consumption generated during a building's operational period, which includes energy consumption for cooling, heating, equipment, lighting, and domestic hot water. The EUI of residential buildings is calculated as follows:

$$EUI = \frac{E_c + E_h + E_e + E_l + E_d}{A} \quad (1)$$

where EUI is the annual building EUI (kWh/(m^2·a)), E_c is the cooling energy consumption (kWh), E_h is the heating energy consumption (kWh), E_e is the equipment energy consumption (kWh), E_l is the lighting energy consumption (kWh), E_d is the domestic hot water energy consumption (kWh), and A is the internal usable area (m^2).

$$E_h = \frac{Q_h}{COP_h} \quad (2)$$

where Q_h is the total annual heating consumption of the building (kWh), and COP_h is the coefficient of performance of the heating system (-).

$$E_c = \frac{Q_c}{COP_c} \quad (3)$$

where Q_c is the total annual cooling consumption (kWh), and COP_c is the coefficient of performance of the cooling system (-).

(2) ITC: The ITC is an important indicator for evaluating the performance of residential buildings. ITC can be evaluated using various methods, with Fanger's Predicted Mean Vote (PMV) and Predicted Percentage of Dissatisfaction (PPD) approaches being the most widely adopted. The PMV and PPD were hourly simulated values for the entire year, and using the PMV would result in excessive cooling or heating; however, the average value of PMV would still show comfort, thereby causing optimization errors. Because the optimization target value is always expressed as a single value in the optimization objectives, this study selected the average PPD over the entire year of the room with the poorest thermal comfort as an optimization objective.

(3) Increment in the total LCC: The economic evaluation of the life cycle of buildings can be divided into static and dynamic evaluation methods based on the consideration of time factors [55]. The static evaluation method does not consider the time factor of funds in economic evaluation, and its calculation is simple and suitable for the rough calculation of solutions, such as the investment payback period, investment return rate, and difference investment payback period methods. Dynamic methods, which account for the time value of funds, yield more accurate results, typically using metrics such as net present value, annual value, investment payback period, and internal rate of return. This study employed a dynamic net present value approach, discounting future cash flows to their present values.

Because the optimized designs of the ULEBs and reference buildings have no significant difference in construction costs, differences exist only in energy-saving materials. This study used the reference building as the benchmark level to calculate the incremental LCC generated by the optimized design and converted it into a present value through net present value as one of the optimization objectives. The LCC was calculated as follows:

$$LCC = C_I + C_o \tag{4}$$

where LCC is the total life-cycle cost (CNY), C_I is the initial investment cost for the building (CNY), and C_o is the cost during the building operation period (CNY).

Because this study focuses on optimizing the design of energy-saving materials, such as the insulation layer of the building envelope and windows, only the cost of the optimized components was considered when calculating the initial investment cost of the building. The calculation formula is as follows:

$$C_I = C_w \cdot V_w + C_r \cdot V_r + C_{wd} \cdot A_{wd} \tag{5}$$

where C_w is the unit price of the external wall insulation material (CNY/m^3), V_w is the volume of the external wall insulation material (m^3), C_r is the unit price of the roof

insulation material (CNY/m^3), V_r is the volume of the roof insulation material (m^3), C_{wd} is the unit price of the energy-saving external window (CNY/m^2), and A_{wd} is the area of the window (m^2).

The cost calculation formula for the operational stage of buildings is as follows:

$$C_o = \sum_{t=1}^{N} C_o(t) \tag{6}$$

$$C_o(t) = \frac{E_e \cdot e_e}{(1+r)^t} \tag{7}$$

where $C_o(t)$ is the discounted value of the cost in the *t*-th year (CNY), E_e is the total annual energy consumption of the building (kWh), e_e is the annual electricity price per kWh of the building (CNY/kWh), and the local electricity price in this study is 0.65 CNY/kWh, *r* is the discount rate (%), and *t* is the building's life cycle, which is 50 years.

$$C = C_{LCC,i} - C_{LCC,ref} \tag{8}$$

where *C* is the incremental cost of building life cycle (CNY), $C_{LCC,i}$ is the total life cycle cost of optimized solution *i* (CNY), and $C_{LCC,ref}$ is the total life cycle cost of the reference building (CNY).

The investigation of residential electricity tariffs in Nanchang and Guangzhou revealed that both cities use tiered pricing systems. In Nanchang, the rate is 0.60 CNY/kWh for annual consumption up to 2160 kWh, 0.65 CNY/kWh for usage between 2161 and 4200 kWh, and 0.90 CNY/kWh for consumption above 4200 kWh. In Guangzhou, the rate is 0.59 CNY/kWh up to 2760 kWh, 0.64 CNY/kWh for usage between 2761 and 6000 kWh, and 0.89 CNY/kWh above 6000 kWh. Calculations showed that all users in the case building fell within the second-tier consumption range in both cities.

In this study, the thickness of the insulation materials was varied to alter the U-value of the non-translucent building envelope structure. Currently, the commonly used building insulation materials are EPS and XPS panels. With the same thickness, the XPS panels have a lower U-value than the EPS panels [56]. However, as external wall insulation

materials, their thermal stability, fire resistance, and air permeability are inferior to those of the EPS panels [56]. Therefore, this study selected EPS panels as the insulation material for the non-translucent building envelope structure of buildings with a material lifespan of 25 years. Through market research on the price of EPS panels, it was determined that the unit price was 240 CNY/m^3. According to the restrictions on the U-value of windows in GB/T51350-2019, this study selected different window types based on their U-values. Aluminum alloy profiles were used for the window frames of the reference building, with a price of 240 CNY/m^2 and a service life of 30 years. It should be noted that parameters such as the U-value of the reference building envelope were derived from actual construction drawings, and certain parameter values may not comply with the requirements specified in GB/T 51350-2019.

2.3.3 Data set acquisition based on the orthogonal test

As the subjects of this study have eight optimization variables and the value ranges of each variable are large, conducting a comprehensive simulation would result in an extremely large workload. Compared with a comprehensive simulation, an orthogonal experimental design can obtain reliable results with fewer tests, thereby significantly reducing the simulation complexity [57]. Therefore, in this study, an orthogonal experimental design was used to design a solution for optimize the variables to obtain data for the predictive model. First, the value range of each optimization variable was selected according to the specifications, and they were divided into five orthogonal-level grades, as listed in Table 5. Then, the orthogonal experimental design table was obtained using SPSS software, and based on the $L_{49}(8^5)$-49 standard test solutions provided by the orthogonal table, each test solution was subjected to a simulation case, and the simulation results were used as the training and test sets for machine learning, which was then used for subsequent prediction and optimization.

Table 5: Horizontal values of the orthogonal design.

Climate zone	Optimization variables	Levels				
		1	2	3	4	5

HSCW	Thickness of the external wall insulation layer (mm)	X_1	70	100	130	160	190
	Thickness of roof insulation layer (mm)	X_2	80	105	130	155	180
	East-facing WWR	X_3	0.1	0.1625	0.225	0.2875	0.35
	South-facing WWR	X_4	0.2	0.2625	0.325	0.3875	0.45
	West-facing WWR	X_5	0.1	0.1625	0.225	0.2875	0.35
	North-facing WWR	X_6	0.15	0.2125	0.275	0.3375	0.4
	Window U-value (W/(m²·K))	X_7	1	1.375	1.75	2.125	2.5
	SHGC	X_8	0.1	0.175	0.25	0.325	0.4
HSWW	Thickness of the external wall insulation layer (mm)	X_1	20	40	60	80	100
	Thickness of roof insulation layer (mm)	X_2	70	80	90	100	110
	East-facing WWR	X_3	0.10	0.15	0.20	0.25	0.30
	South-facing WWR	X_4	0.20	0.25	0.30	0.35	0.40
	West-facing WWR	X_5	0.10	0.15	0.20	0.25	0.30
	North-facing WWR	X_6	0.15	0.2125	0.275	0.3375	0.40
	Window U-value (W/(m²·K))	X_7	1	1.375	1.75	2.125	2.5
	SHGC	X_8	0.10	0.15	0.20	0.25	0.30

2.3.4 Sensitivity analysis

A sensitivity analysis was conducted to assess the effects of the design variables on building performance. Regression methods are widely used due to their simplicity and efficiency [58]. Many sensitivity indicators are based on regression analysis, including standardized regression coefficients, partial correlation coefficients, standardized rank regression coefficients, and Partial Rank Correlation Coefficients (PRCC) [36]. PRCC is typically applied to nonlinear and monotonic input-output relationships [59]. This reflects both the direction and magnitude of the impact of the optimization variables on the objectives. The direction of the influence is indicated by the sign, which is either

positive or negative. The absolute value of the PRCC indicates the strength of the influence, with larger values representing greater impact.

2.4 ANN prediction model

This study employed a metamodel to enhance the optimization efficiency. Metamodels for building performance optimization are constructed using algorithms that learn input-output variable relationships, using simulation data to build alternative models for performance prediction. Common machine learning algorithms for metamodels include ANN, GBDT, support vector machines, and multiple linear regression. Given ANN's high accuracy in building performance studies and its widespread use (Table 1), this study used MATLAB's ANN toolbox to generate the metamodel. Prior to machine learning on orthogonal data, the dataset was randomly split into an 80% training set and a 20% test set; the former trained the metamodel, and the latter validated its quality. The ANN structure includes input, hidden, and output layers, with the hidden layer node counts determined using Equation (9):

$$h = \sqrt{m + n} + a \tag{9}$$

where h is the number of nodes in the hidden layer, m is the number of nodes in the input layer, n is the number of nodes in the output layer, and a is the adjustment constant, which is between 1 and 10.

The ANN model's prediction performance was evaluated using the coefficient of determination (R^2), Mean Squared Error (MSE), and Mean Absolute Percentage Error (MAPE). R^2, which ranges from 0 to 1, assesses metamodel prediction accuracy, with values closer to 1 indicating better accuracy. MSE calculates the average squared difference between the actual and predicted values, making it sensitive to outliers (larger errors disproportionately impact the MSE). MAPE serves as a prediction accuracy indicator: <10% is highly accurate, 11–20% is good, 21–50% is reasonable, and >51% is inaccurate. The mathematical formulas for these metrics are provided in Equations (10) - (12) [60]:

$$R^2 = 1 - \frac{\sum_{i=1}^{n}(y_i - \hat{y}_i)^2}{\sum_{i=1}^{n}(y_i - \overline{y})^2} \tag{10}$$

$$MSE = \frac{\sum_{i=1}^{n}(y_i - \hat{y}_i)^2}{n} \tag{11}$$

$$MAPE = \frac{100\%}{n}\sum_{i=1}^{n}\left|\frac{y_i - \hat{y}_i}{y_i}\right| \tag{12}$$

where y_i is the true value, $\overline{y}$ is the average of all true values, $\hat{y}_i$ is the predicted value of the model, and n is the sample size of the training set.

The number of neurons in the hidden layer was determined using Equation (9), yielding values within the range [5,13]. The number of nodes in the input and output layers was set to eight and three, respectively, corresponding to the number of optimization variables and target outputs. The input and output parameters from the simulation were mapped to the ANN's layers to ensure physically meaningful neuron behavior. Subsequently, an error analysis was conducted for the ANN model with varying numbers of hidden layer neurons, and the results are summarized in Table 6. The 8-10-3 network architecture demonstrated the lowest prediction error and highest R^2 value in both climate zones, as shown in Table 6. Therefore, a hidden layer with ten neurons achieved a minimal model error. Furthermore, when the number of neurons in the neural network varied by ±10%, the fluctuation of the model's R^2 value was only within 0.02, indicating that the predictive model of the ANN had strong robustness. Additionally, key hyperparameters were configured to reduce the risk of overfitting: a maximum of 500 training epochs and a learning rate of 0.01 were used.

Table 6: Comparison of network errors with different hidden layer neuron counts.

Case	Hidden Layer Count	MSE	R^2
Nanchang	5	0.05289	0.94785
	6	0.05398	0.94968
	7	0.05015	0.95299
	8	0.04765	0.93251
	9	0.03451	0.93497
	10	0.03042	0.97422

	11	0.06921	0.94186
	12	0.08701	0.94308
	13	0.09768	0.94129
	5	0.05771	0.92171
	6	0.06193	0.93905
	7	0.05566	0.94179
	8	0.04079	0.94821
Guangzhou	9	0.02831	0.94865
	10	0.02164	0.95253
	11	0.06218	0.93747
	12	0.07540	0.92502
	13	0.09463	0.93389

Random perturbation tests were performed on the input parameters of the ANN model to evaluate its robustness. The perturbation ranges for each parameter were specified as follows: the insulation layer thickness was perturbed by ±5%, the WWR was perturbed by ±3%, the external window U-value was perturbed with uniform noise of ±0.3, and the solar heat gain coefficient was perturbed with uniform noise of ±0.05. Based on these perturbation ranges, MATLAB was used to randomly add perturbation values to the input parameters. The MAPE results before and after the perturbation were analyzed to evaluate the model's robustness. As shown in Table 7, the variation range of the MAPE values before and after perturbation was within 5%, which suggests that the model has strong robustness.

Table 7: Test results of ANN model robustness.

Case	Optimization objective	Initial MAPE value	Final MAPE value	Comparison results
Nanchang	EUI	3.0%	3.7%	0.7%
	PPD	2.8%	3.2%	0.4%
	LCC	9.7%	12.8%	3.1%
Guangzhou	EUI	2.9%	3.6%	0.7%
	PPD	1.6%	2.4%	0.8%
	LCC	7.6%	11.4%	3.8%

2.5 NSGA-II-MOPSO multi-objective optimization

2.5.1 NSGA-II-MOPSO optimization procedure

The hybrid NSGA-II-MOPSO algorithm integrated the elitist preservation mechanisms of NSGA-II, specifically non-dominated sorting and crowding distance estimation, with the adaptive velocity-position update mechanism of MOPSO to overcome the limitations inherent in single-algorithm approaches. While NSGA-II demonstrated slow convergence in complex optimization landscapes, MOPSO was prone to premature convergence owing to its excessive emphasis on local exploitation. By synergistically combining these complementary strengths, the hybrid framework achieved a balanced trade-off between global exploration and local exploitation [61]. The hybrid framework employed a parallel fusion strategy for NSGA-II and MOPSO. In each iteration, NSGA-II's genetic operations (selection, crossover, mutation) and MOPSO's particle velocity/position updates were performed simultaneously on the parent population. Through a shared information pool, this fusion enhanced NSGA-II's local search capability while expanding the search directions of MOPSO particles. This dual subpopulation strategy effectively alleviated the stagnation in NSGA-II and prevented the premature convergence in MOPSO.

To ensure compatibility between the two algorithms, a preprocessing step aligned their operational mechanisms by mapping MOPSO's particle position updates of MOPSO onto the generational update framework of NSGA-II, treating updated particles as offspring and original individuals as parents. Because NSGA-II lacks a velocity component, new individuals were initialized with zero velocity. A template for storing individual optima was added to NSGA-II, whereas MOPSO's global best was selected from the parent population to maintain consistency. The algorithm began by initializing the key parameters with a population size of 50 and a maximum of 100 generations, followed by objective function evaluation, non-dominated sorting, and concurrent execution of both sub-algorithms until convergence. This parallel architecture enabled real-time information exchange, enhancing the convergence speed and solution diversity [62]. Table 8 lists the initial parameter settings of the three optimization

algorithms. As shown in Figure 4, the hybrid approach merged the parent population P_t with offspring populations Q_{t1} from NSGA-II and Q_{t2} from MOPSO to form a combined population R_t. After fast non-dominated sorting, the first N optimal solutions were selected to create the next parent population P_{t+1}, ultimately yielding the Pareto-optimal front upon termination.

Table 8: Initial parameters for NSGA-II, MOPSO, and the hybrid algorithm.

Algorithm	Population size	Maximum number of iterations	Crossover proportion	Mutation probability	Mutation proportion	Individual learning factor	Global learning factor	Maximum weight coefficient	Minimum weight coefficient
NSGA-II algorithm	50	100	0.8	0.05	0.2	-	-	-	-
MOPSO algorithm	50	100	-	-	-	1	2	0.8	0.1
Hybrid algorithm	50	100	0.8	0.05	0.2	1	2	0.8	0.1

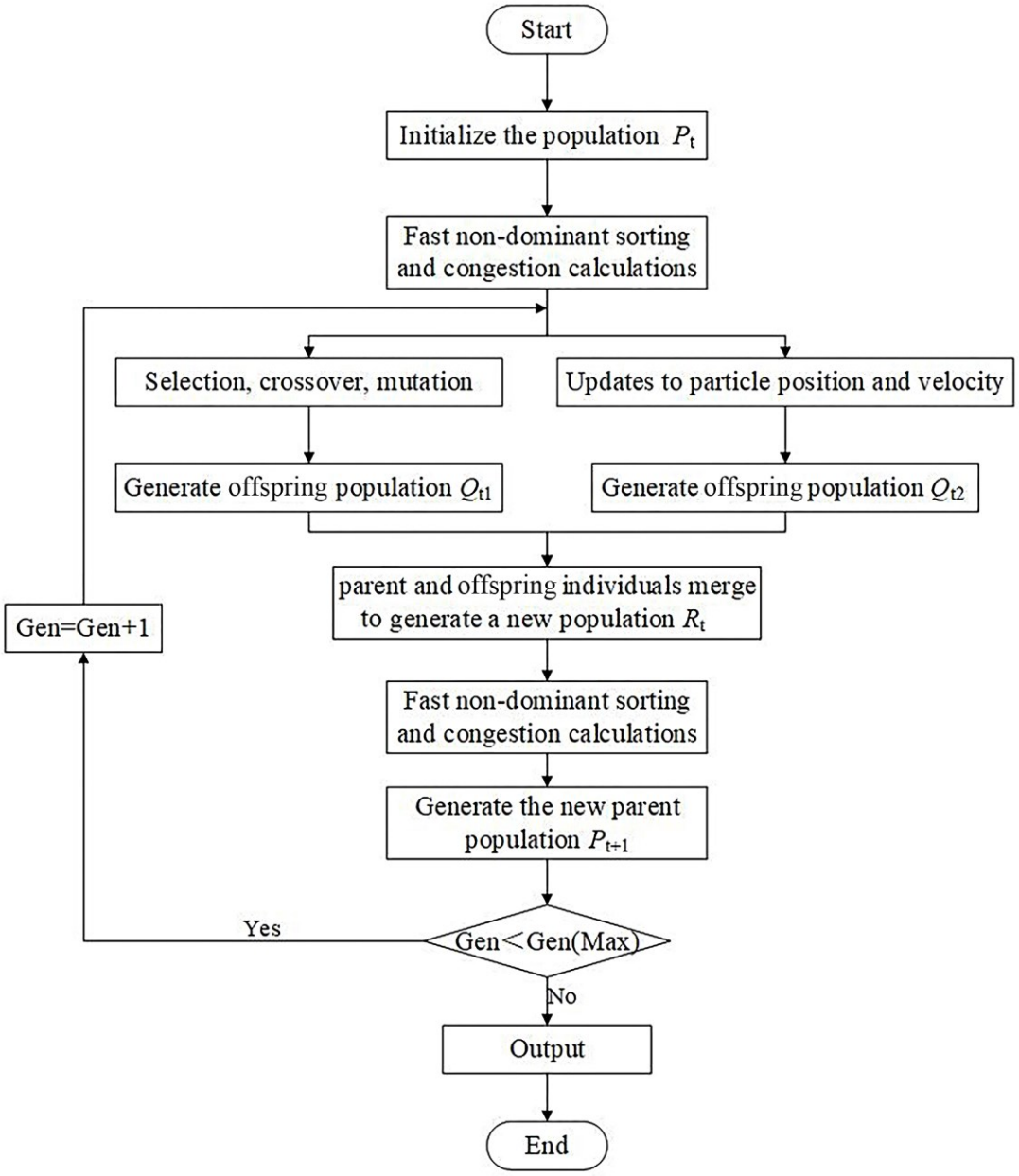

Figure 4. NSGA-II-MOPSO flow.

2.5.2 Performance indicators of optimization algorithms

(1) The hypervolume (HV) index was applied to compare the performance of the three algorithms, which was used to evaluate the efficiency of the optimization method [63,64]. The hypervolume metric was used to evaluate the extent to which the target space was covered by an approximate set. Its value represents the volume of the hypercube formed by the individuals in the solution set and the reference point in the target space. If the HV value of the non-dominated solution set is larger, it indicates that

this solution set is closer to the real Pareto frontier in terms of convergence and diversity. The calculation formula is as follows:

$$HV(X,P) = \bigcup_{i=1}^{|X|} v_i \tag{13}$$

where X represents the non-dominated solution set obtained by the algorithm, P is the reference point, $|X|$ is the cardinality of the non-dominated solution set, and v_i is the volume of the hypercube formed by the diagonal of the space between solution x_i in the non-dominated solution set and the reference point.

(2) The Inverted Generational Distance (IGD) is an indicator that can simultaneously evaluate the convergence and diversity of algorithms [65]. It is used to calculate the average Euclidean distance between all solutions in the true Pareto front and the non-dominated solutions obtained by the solving algorithm. The IGD metric quantifies the proximity between the algorithm-generated and true Pareto fronts, where a lower value indicates better convergence to the optimal front and a better solution distribution. The calculation formula is as follows:

$$IGD(X,P^*) = \frac{\sum_{x^* \in P^*} d(x^*,X)}{|P^*|} \tag{14}$$

where P^* is a solution set on the Pareto front, $d(x^*,X)$ is the minimum Euclidean distance from x^* in the reference solution set P^* to the solutions in X, $|P^*|$is the cardinality of the solution set P^*.

(3) The Spacing (Sp) performance measure quantifies the distribution of solutions in the obtained approximation of the Pareto front; a value of zero indicates perfectly uniform spacing among solutions, and it can be computed as [66]:

$$S_p = \sqrt{\frac{1}{|P|}\sum_{i=1}^{|P|}(\bar{d} - d_i)^2} \tag{15}$$

where d_i and $\bar{d}$ are defined as: $d_i = \min_{i \neq j} \sum_{k=1}^{M} |f_k^i - f_k^j|$ and $\bar{d} = \frac{\sum_{i=1}^{|P|} d_i}{|P|}$.

2.5.3 Utopian point method

The Pareto optimal solution set obtained via optimization algorithms represents a collection of non-dominated decision solutions rather than a single optimal outcome. To facilitate decision-making, this study employed the utopian point method—a MOO technique that identifies the optimal compromise solution by minimizing the distance between candidate solutions and the utopian point. Defined as the theoretical combination of each objective's individual optimal values on the Pareto frontier, the utopian point serves as a benchmark for evaluating solution optimality. Taking the three-objective example of this study, the distance between each point in the Pareto set and the utopian point was calculated using Equation (16):

$$U_n = \left[\left(\frac{\alpha_p - \alpha_{p\_best}}{\alpha_{p\_best}} \right)^2 + \left(\frac{\beta_p - \beta_{p\_best}}{\beta_{p\_best}} \right)^2 + \left(\frac{\gamma_p - \gamma_{p\_best}}{\gamma_{p\_best}} \right)^2 \right]^{1/2} \quad (16)$$

where α_{p_best} is the optimal value of BEC, β_{p_best} is the optimal value of ITC, γ_{p_best} is the optimal value of the LCC, (α_p, β_p, γ_p) is the coordinates of the corresponding Pareto front point.

After calculating the distance between each point in the optimal solution set and the utopian point, the point with the minimum distance was selected as the optimal solution.

$$U_{\text{opt}} = \min(U_{\text{n}}) \quad (17)$$

This study took the calculation results of the reference building design parameters as the reference point and normalized the reference point and the Pareto optimal solution set obtained in each iteration to prevent the influence of large-scale dimensional data on the calculation results. The normalized index of the reference point after normalization was (1, 1, 1).

3. Results and discussions

3.1 Impact of optimization variables on optimization objectives

Figure 5 presents the correlation analysis results between the optimization variables and objectives via PRCC. As shown in Figure 5(a), the external wall insulation thickness was strongly negatively correlated with EUI (PRCC = − 0.58) and PPD (PRCC = − 0.41), but positively correlated with LCC (PRCC = 0.32). Its influence on objectives surpassed that of roof insulation thickness. Roof insulation thickness was weakly negatively correlated with EUI (PRCC = − 0.16) and slightly positively correlated with LCC (PRCC = 0.09), having a lower impact on ITC. For all directions, WWR positively correlated with objectives, with south-facing and north-facing WWR having greater impacts. S-WWR shows PRCCs of 0.38 (EUI), 0.43 (PPD), 0.61 (LCC); N-WWR has 0.25 (EUI), 0.03 (PPD), 0.48 (LCC), due to large south and north facade areas. The external window U-value positively correlated with the BEC and ITC but negatively with the LCC. SHGC shows the opposite pattern, negatively correlating with BEC and ITC, and weakly positively with LCC.

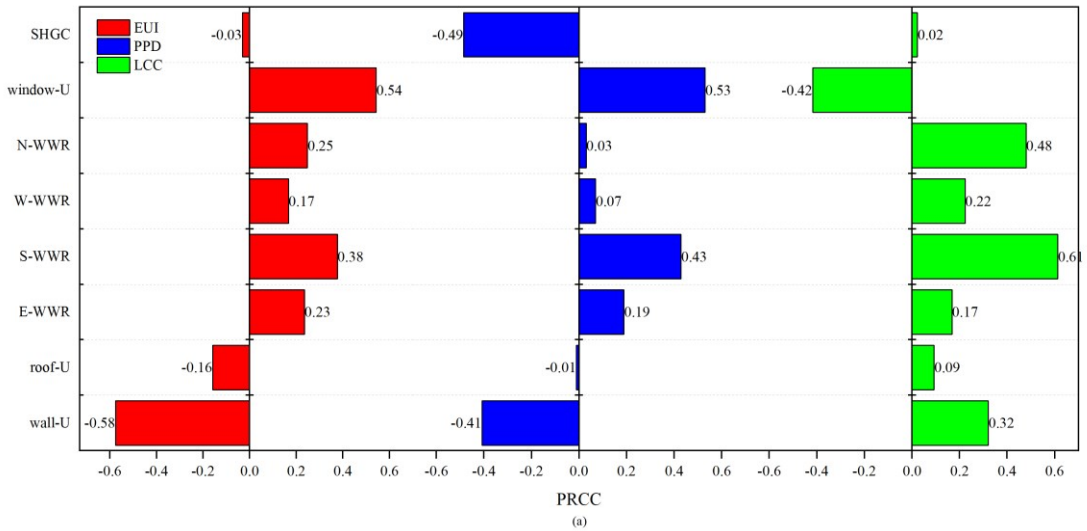

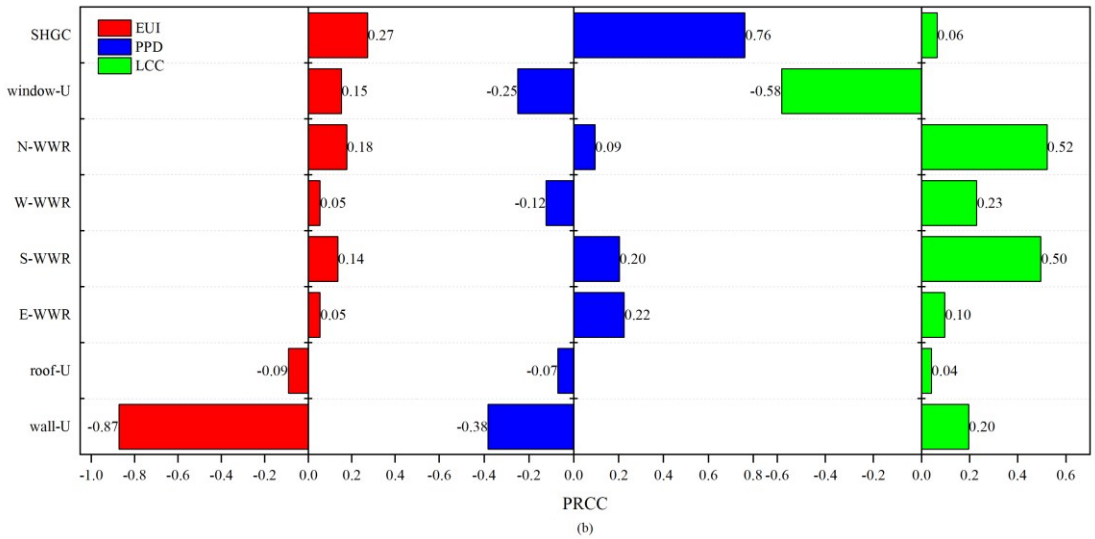

Figure 5. Results of redundancy analysis: (a) Nanchang and (b) Guangzhou.

In Figure 5(b), external wall insulation (wall-U) strongly negatively correlates with EUI (PRCC = −0.87) and moderately with PPD (PRCC = −0.38), and positively with LCC (PRCC = 0.20), showing greater influence than roof insulation (roof-U), which has weak negative correlations with EUI (PRCC = −0.09) and PPD (PRCC = −0.07), and a slight positive with LCC (PRCC = 0.04). Among WWRs, N-WWR and S-WWR have higher impacts: N-WWR (PRCC = 0.18 EUI, 0.09 PPD, 0.52 LCC); S-WWR (PRCC = 0.14 EUI, 0.20 PPD, 0.50 LCC). W-WWR weakly positively correlates with EUI (0.05), negatively with PPD (−0.12), and positively with LCC (0.23); E-WWR shows PRCCs of 0.05 (EUI), 0.22 (PPD), and 0.10 (LCC). Window-U positively correlates with EUI (0.15), negatively with PPD (−0.25), and strongly negatively with LCC (−0.58). SHGC exhibits the reverse: positive with EUI (0.27) and strongly positive with PPD (0.76), and weakly positive with LCC (0.06).

3.2 ANN prediction and accuracy analysis

Figure 6 illustrates the comparison between the predicted values from the ANN model and the actual values. The ANN model exhibited high accuracy in predicting EUI, PPD, and LCC. For the Nanchang case, the R^2 values for these three optimization objectives were 0.959, 0.978, and 0.988, respectively. In the Guangzhou case, the corresponding

R^2 values were 0.980, 0.942, and 0.972. These results indicated that the prediction models performed well and could be employed as the fitness function in the subsequent MOO algorithm.

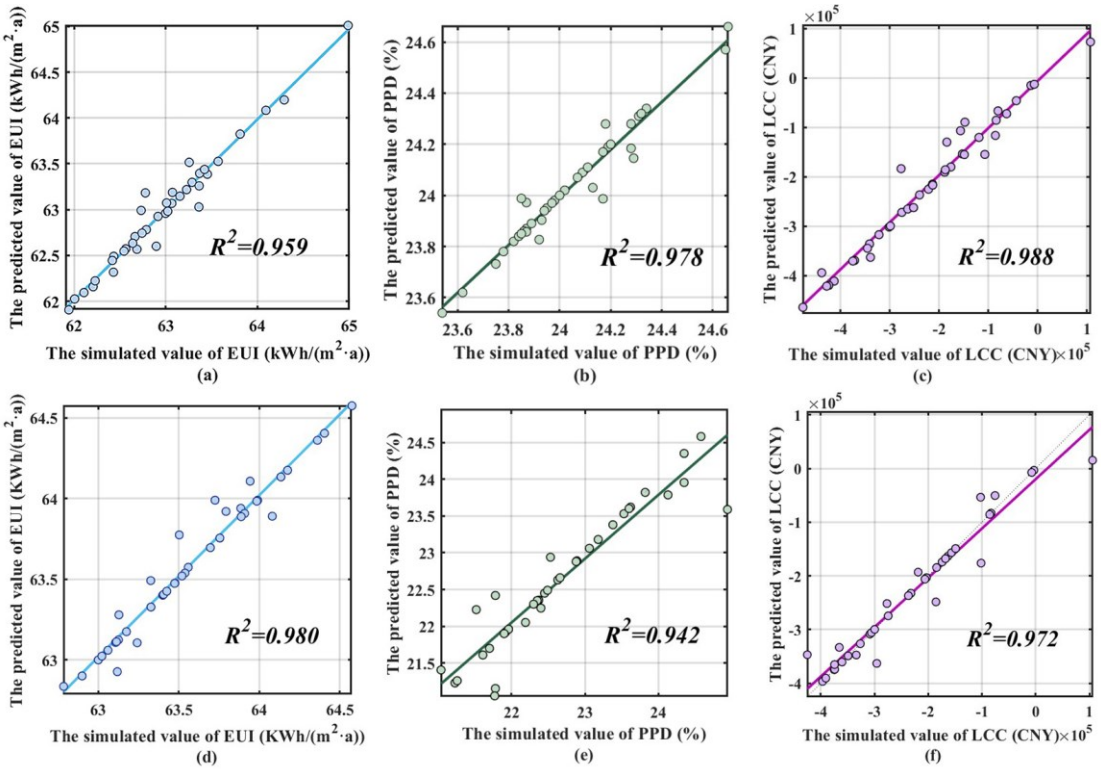

Figure 6. Prediction results of the objective function in the ANN model.

3.3 Performance comparison of optimization algorithms

Hypervolume results of the two cases were presented in Figure 7. In Figure 7(a), during the initial stage, as function evaluations increased, the hypervolume index of each algorithm also rose. The hybrid NSGA-II-MOPSO algorithm's HV value tended to stabilize at 800 function evaluations, while the NSGA-II and MOPSO algorithms began to stabilize their HV values at 1700 and 1150 function evaluations, respectively. This indicated that the hybrid NSGA-II-MOPSO algorithm could quickly obtain the Pareto optimal solution set with fewer iterations. Additionally, the final hypervolume values of the three optimization algorithms were 0.648 (NSGA-II), 0.640 (MOPSO), and 0.676 (NSGA-II-MOPSO), respectively. In Figure 7(b), the hybrid algorithm's HV value tended to stabilize at 400 function evaluations, whereas the NSGA-II and MOPSO algorithms began to stabilize their HV values at 900 and 700 function evaluations,

respectively. This also indicated that the hybrid NSGA-II-MOPSO algorithm could quickly obtain the Pareto optimal solution set with fewer iterations. The final hypervolume values of the three optimization algorithms here were 0.665 (NSGA-II), 0.659 (MOPSO), and 0.668 (NSGA-II-MOPSO), respectively. Therefore, the MOO performance of the hybrid NSGA-II-MOPSO algorithm proposed in this study was superior to that of the other two algorithms in terms of both diversity and convergence.

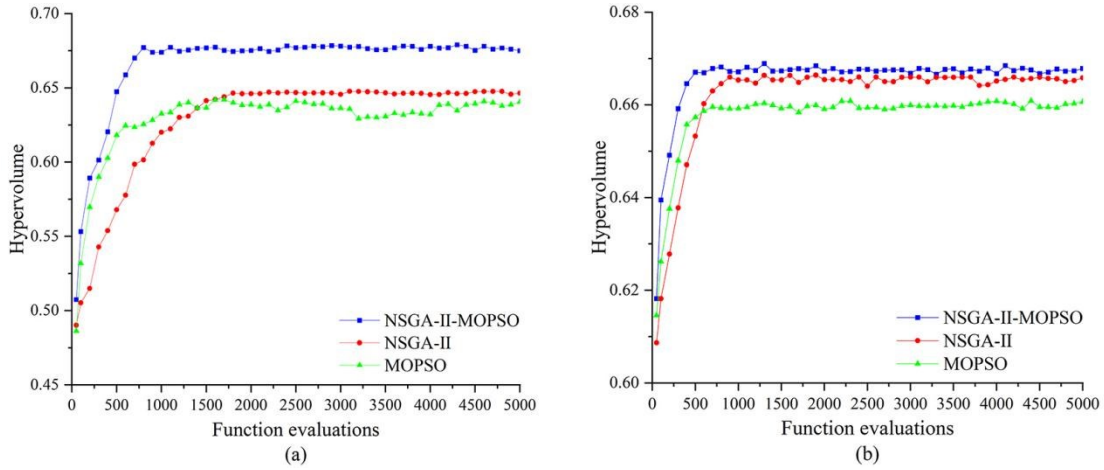

Figure 7. Hypervolumes of each optimization algorithm: (a) Nanchang and (b) Guangzhou.

Table 9 presents the IGD results, showing that the hybrid NSGA-II-MOPSO algorithm outperformed NSGA-II and MOPSO in both cases. The hybrid algorithm achieved IGD values of 0.02133 in Nanchang and 0.00959 in Guangzhou, compared to 0.02413 and 0.01172 for NSGA-II, and 0.02638 and 0.01394 for MOPSO, demonstrating its superior convergence. Table 10 illustrates the spacing metric results, further confirming the hybrid algorithm's advantage with values of 0.03671 in Nanchang and 0.02104 in Guangzhou, as opposed to 0.04052 and 0.02605 for NSGA-II, and 0.03849 and 0.02370 for MOPSO, indicating better solution uniformity. Overall, the hybrid NSGA-II-MOPSO algorithm exhibited enhanced performance in terms of both convergence and solution diversity across the two climate zones when compared to NSGA-II and MOPSO.

Table 9: Results of IGD metric for NSGA-II, MOPSO, and proposed hybrid NSGA-II-MOPSO algorithms.

Case	IGD metric		
	NSGA-II	MOPSO	NSGA-II-MOPSO
Nanchang	0.02413	0.02638	0.02133
Guangzhou	0.01172	0.01394	0.00959

Table 10: Results of spacing metric for NSGAII, MOPSO, and proposed hybrid NSGA-II-MOPSO algorithms.

Case	Spacing metric for the optimal solution		
	NSGA-II	MOPSO	NSGA-II-MOPSO
Nanchang	0.04052	0.03849	0.03671
Guangzhou	0.02605	0.02370	0.02104

3.4 MOO results of the hybrid algorithm

The distribution of Pareto optimal solutions for the MOO of ultra-low energy residential buildings using three optimization algorithms is shown in Figure 8. In Nanchang, the hybrid algorithm yielded the broadest EUI interval [61.53, 63.56 kWh/(m²·a)] compared to NSGA-II [61.73, 63.42] and MOPSO [61.75, 63.16], while narrowing the PPD range to [23.27, 24.18%] and achieving the largest LCC saving interval [−479,138.24, −49,230.42 CNY]. In Guangzhou, the hybrid algorithm maintained similar EUI ranges but remarkably concentrated PPD values at [23.72, 23.72%] and expanded the LCC saving interval to [−673,341.35, −243,555.87 CNY], outperforming other algorithms. This performance originated from the hybrid algorithm's integration of NSGA-II's global exploration and MOPSO's fast local convergence, balancing solution diversity and precision: it expanded the energy-optimized solution space in Nanchang, achieved precise thermal comfort optimization in Guangzhou, and showed consistent economic advantages across climates, verifying its superiority in building MOO design. Thus, the hybrid algorithm's calculation results were used to analyze optimized design solutions in the following section.

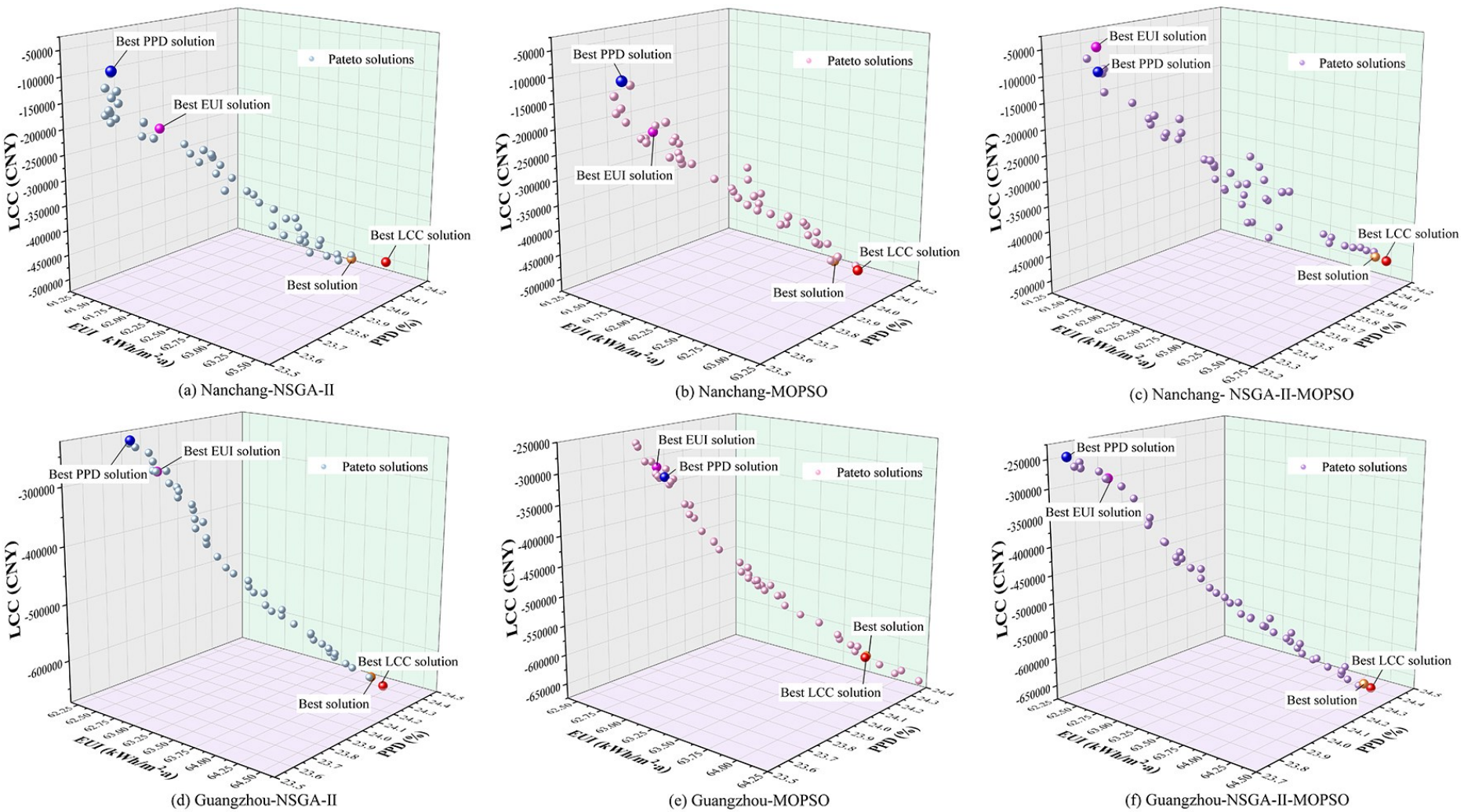

Figure 8. Pareto optimal solutions distribution for MOO of ultra-low energy residential buildings.

In Nanchang, the buildings achieved an EUI between 61.25 and 63.75 kWh/(m²·a), with the average PPD value for rooms with the poorest thermal comfort throughout the year ranging from 23.2% to 24.2% and LCC savings between 50,000 and 500,000 CNY. In Guangzhou, the EUI of buildings fell between 62.38 and 64.20 kWh/(m²·a), the corresponding average PPD value for the least thermally comfortable rooms ranged from 23.7% to 24.4%, and LCC savings varied from 240,000 to 670,000 CNY. All solutions obtained in this study showed an EUI below 65 kWh/(m²·a), meeting the design requirements for ultra-low energy residential buildings. Compared with the reference model, the PPD value for indoor thermal comfort across all solutions was lower. The LCC, which combined initial investment cost and operating cost, was ≤ 0, indicating that the buildings achieved economic savings over their life cycle. Additionally, the cost increment of all design solutions was less than 0. To further illustrate the trade-offs among the three objectives, a parallel coordinate radar chart of the non-dominated solutions is presented in Figure 9.

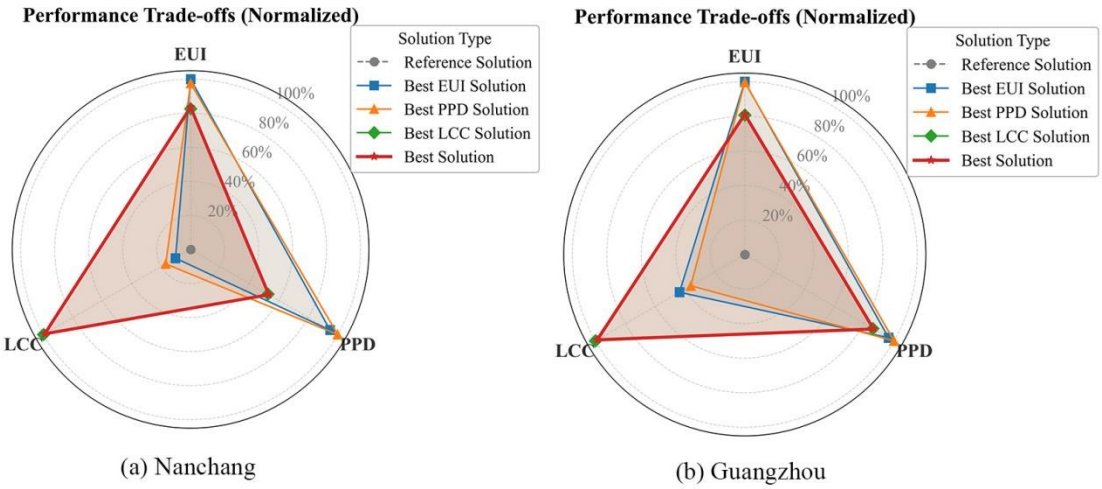

Figure 9. Normalized radar charts illustrating MOO performance trade-offs (EUI, LCC, PPD) for the case building: (a) Nanchang and (b) Guangzhou.

Based on the Pareto optimal solution set, the optimal insulation layer thickness for building external walls in ultra-low energy residential buildings in Nanchang ranged from 150 to 190 mm, with corresponding U-values between 0.15 and 0.18 W/(m²·K); the optimal value of the insulation layer thickness of the roof mainly fallen within the

range of 150 to 180 mm, and the corresponding U-value was between 0.15 and 0.19 W/(m²·K). The optimal values of the WWR for each orientation of the building were all around the lower limit of the WWR requirement. The external window U-value was mainly at around 1 or 2.5 W/(m²·K), and the SHGC value was mainly between 0.3 and 0.4. Due to the conflicting relationship among the three optimization objectives, the values of the optimization variables were relatively scattered. For the Guangzhou case, the external wall insulation thickness concentrated at 20 and 100 mm, with corresponding U-values of 0.8 and 0.3 W/(m²·K). The roof thickness ranged from 90 to 110 mm, corresponding to U-values between 0.25 and 0.3 W/(m²·K). The optimal WWRs were similar to those in Nanchang, all approaching the lower limit of the required WWR. The external window U-values ranged from 1 to 1.5 W/(m²·K), and the SHGCs were between 0.2 and 0.3. Due to differences in climate zones, the optimization of building U-values varies significantly. In HSCW regions, exterior wall U-values must be lower to balance summer heat insulation and winter heat retention. Meanwhile, Nanchang, a typical HSCW city, optimizes exterior window U-values by first meeting local energy requirements to cut costs. By contrast, Guangzhou (HSWW region) has much lower exterior wall insulation/heat retention needs—focusing only on summer heat insulation with minimal winter needs. Thus, to meet energy standards and control costs, a higher U-value works for Guangzhou's exterior walls, avoiding unnecessary high-performance insulation investment.

3.5 Optimal solutions for ultra-low energy residential buildings in case cities

The simulation results for the reference model in Nanchang showed that the total annual energy consumption of the building's equipment and lighting was 66,621.18 kWh, the cooling energy consumption was 57,842.31 kWh, the heating energy consumption was 41,200.57 kWh, and the EUI of the building was 73.11 kWh/(m^2·a). The thermal comfort of the reference model showed that the average PPD value of the room with the poorest thermal comfort in the building throughout the year was 25.2%. The total annual energy consumption of the building and the unit price of the building's materials mentioned above were used to calculate the LCC of the reference model, which was

3047,213.03 CNY. In Guangzhou, the reference building exhibited an annual total energy consumption of 66,621.18 kWh for equipment and lighting, with cooling energy consumption at 85,519.73 kWh, heating energy consumption at 10,644.79 kWh, and an EUI of 71.84 kWh/(m²·a). The average PPD value for the room with the poorest annual thermal comfort was 28.59%, and the LCC calculated from the annual energy consumption and material unit prices was 2,970,201.28 CNY. Neither reference model met the energy requirements of ULEBs, necessitating further design optimization of the building envelope to derive optimal solutions.

Through the screening of the Pareto optimal solution set, the best EUI, PPD and LCC solutions are obtained, as shown in Table 11. The results were compared with those of the reference model. In Nanchang, compared with the reference model solution, the best EUI solution reduced energy consumption by 15.8%, the best PPD solution reduced indoor dissatisfaction by 7.6%, and the best LCC solution saved 479,138 CNY. In Guangzhou, the best EUI solution reduced energy consumption by 13.2%, the best PPD solution reduced indoor dissatisfaction by 17.0%, and the best LCC solution saved 673,341 CNY. While all optimization solutions met the ultra-low energy building codes, one of the optimal design solutions, though achieving good results in a specific building performance indicator, might fail to meet the desired outcomes for its other performance indicators.

Table 11: Comparison of the optimization solutions.

Case	Design variables	Unit	Reference solution	Best EUI solution	Best PPD solution	Best LCC solution	Best solution
Nanchang	X_1	mm	30	190	154	70	87
		W/(m²·K)	0.649	0.150	0.176	0.348	0.291
	X_2	mm	40	180	180	126	128
		W/(m²·K)	0.620	0.150	0.150	0.223	0.220
	X_3	–	0.02	0.35	0.35	0.10	0.10
	X_4	–	0.40	0.20	0.20	0.20	0.20
	X_5	–	0.02	0.25	0.10	0.10	0.10
	X_6	–	0.25	0.15	0.23	0.15	0.15
	X_7	W/(m²·K)	5.8	1.0	1.0	2.5	2.5
	X_8	–	0.75	0.32	0.4	0.1	0.1
	Y_1	kWh/(m^2·a)	73.11	61.53 (−15.8%)	61.81 (−15.5%)	63.55 (−13.1%)	63.43 (−13.2%)
	Y_2	%	25.19	23.37 (−7.2%)	23.27 (−7.6%)	24.18 (−4.0%)	24.17 (−4.1%)
	Y_3	CNY	0	−49230.4	−81226.8	−479138	−475087
Guangzhou	X_1	mm	30	100	100	20	20
		W/(m²·K)	0.649	0.3	0.3	0.8	0.8

X_2	mm	40	110	110	87	84
	W/(m²·K)	0.620	0.25	0.25	0.315	0.325
X_3	–	0.02	0.10	0.30	0.10	0.10
X_4	–	0.40	0.20	0.20	0.20	0.20
X_5	–	0.02	0.10	0.11	0.10	0.10
X_6	–	0.25	0.15	0.15	0.15	0.15
X_7	W/(m²·K)	5.8	1.0	1.0	2.5	2.39
X_8	–	0.75	0.19	0.30	0.27	0.26
Y_1	kWh/(m²·a)	71.84	62.38 (−13.2%)	62.41 (−13.1%)	64.21 (−10.6%)	64.16 (−10.7%)
Y_2	%	28.59	23.90 (−16.4%)	23.72 (−17.0%)	24.41 (−14.6%)	24.39 (−14.7%)
Y_3	CNY	0	−294482	−243556	−673341	−665024

The best solution derived via the utopian point method comprehensively considers three building performance indicators, as shown in Table 11. The best solution for Nanchang cut EUI by 13.2%, lowered average PPD dissatisfaction by 4.1%, and saved 475,087 CNY in LCC. Comparing envelope design parameters across four solutions with the reference model showed several findings. First, thicker external wall and roof insulation reduced EUI. Second, reducing WWR in all orientations was beneficial because the external window U-value exceeded that of external walls. Third, the external window U-value greatly impacted LCC. Larger U-values led to lower PPD. Finally, a larger window SHGC lowered EUI. For Guangzhou, the best solution reduced EUI by 10.7%, PPD by 14.7%, and saved 665,024 CNY in LCC. Examining design parameters across five scenarios revealed: the best EUI solution, via thicker insulation and lower U-values, cut EUI by 13.2%; the best PPD solution, through adjusting window U-values, reduced PPD by 17.0%; the best LCC and best solutions traded off variables for cost savings, with the best solution's LCC (−665,024 CNY) balancing better with EUI and PPD than the best LCC solution's (−673,341 CNY). The best solutions in Nanchang and Guangzhou showed climate-specific trade-offs: thicker insulation and lower WWR reduced EUI by 13.2% in Nanchang, while balancing window U-value and SHGC minimized PPD and LCC. In Guangzhou, prioritizing low U-values and SHGC cut EUI by 10.7% and PPD by 14.7%, with the best solution balancing LCC savings against energy and comfort better than the pure cost-optimized case. These results highlight the importance of tailoring envelope parameters to regional thermal demands for holistic performance optimization.

4. Conclusions

In light of the promotion of ultra-low energy residential buildings in the southern region of China, this study proposed an MOO method for building design based on the hybrid NSGA-II-MOPSO algorithm. By taking BEC, ITC, and LCC as the optimization objectives, an orthogonal experimental design was conducted on eight variables, including the external wall U-value, roof U-value, WWR in each direction (east, south, west, and north), external window U-value, and SHGC. The orthogonal experimental

data were used to construct an ANN prediction model for the optimization objectives. Based on this prediction model, an efficient hybrid machine learning algorithm that combines NSGA-II and MOPSO was developed for the case building optimization design. The corresponding optimized design solutions were obtained. The main conclusions are as follows:

(1) The ANN model exhibited high accuracy in predicting EUI, PPD, and LCC. For the Nanchang case, the R^2 values for the three objectives were 0.959, 0.978, and 0.988; in the Guangzhou case, they were 0.980, 0.942, and 0.972. The ANN model could be used as the fitness function in multi-objective optimization. Performance indicators of the hybrid NSGA-II-MOPSO, NSGA-II, and MOPSO algorithms were calculated. In the Nanchang case, HV values were 0.648 (NSGA-II), 0.640 (MOPSO), and 0.676 (hybrid); in the Guangzhou case, they were 0.665 (NSGA-II), 0.659 (MOPSO), and 0.668 (hybrid). The hybrid algorithm achieved IGD values of 0.02133 (Nanchang) and 0.00959 (Guangzhou), outperforming NSGA-II (0.02413, 0.01172) and MOPSO (0.02638, 0.01394) in convergence. Spacing metrics further confirmed its advantage: 0.03671 (Nanchang) and 0.02104 (Guangzhou) versus NSGA-II (0.04052, 0.02605) and MOPSO (0.03849, 0.02370), indicating better solution uniformity. Overall, the hybrid NSGA-II-MOPSO algorithm showed superior convergence and solution diversity in both climate zones compared to the single algorithms.

(2) Based on the hybrid algorithm, the optimized design parameter ranges for ultra-low energy residential buildings in Nanchang were as follows: external wall and roof U-values were controlled at 0.15–0.18 and 0.15–0.19 W/(m²·K), respectively; WWR in all orientations ranged from 0.1 to 0.25; external window U-values were set at approximately 1 or 2.5 W/(m²·K); and SHGC values were controlled between 0.3 and 0.4. For Guangzhou, the optimized parameters include external wall U-values (0.3 and 0.8 W/(m²·K)), roof U-values (0.25–0.30 W/(m²·K)), and WWRs similar to Nanchang's, approaching the lower limit of requirements. External window U-values ranged from 1 to 1.5 W/(m²·K), with SHGC values between 0.2 and 0.3.

(3) The best solution derived via the utopian point considered three building performance indicators. For Nanchang, key parameters were: external wall U-value 0.29 W/(m²·K), roof U-value 0.22 W/(m²·K), east/west/north WWR 0.1/0.1/0.15, south WWR 0.2, external window U-value 2.5 W/(m²·K), and SHGC 0.1. Compared to the reference model, this reduced EUI by 13.2% to 63.43 kWh/(m²·a), average PPD by 4.1% to 24.17%, and saved LCC by 475,087 CNY. For Guangzhou, the solution featured external wall U-value 0.8 W/(m²·K), roof U-value 0.325 W/(m²·K), the same WWR values (east/west/north 0.1/0.1/0.15, south 0.2), window U-value 2.39 W/(m²·K), and SHGC 0.26. This achieved a 10.7% EUI reduction to 64.16 kWh/(m²·a), 14.7% PPD reduction to 24.39%, and LCC savings of 665,024 CNY.

This study focused on southern China's ultra-low energy residential buildings with relatively simple spatial forms. Before generalizing this approach to more complex building types like ultra-low energy public buildings, further investigation is needed, including adaptive adjustments to design parameters and optimization goals based on specific building characteristics. Additionally, implementing research findings in practice requires significant financial investment, which currently limits the validation and refinement of theoretical results through practical application. Future research could explore additional strategic possibilities, such as applying other deep learning algorithms to classify complex real-world problems, to further advance these research directions.

Declarations of interest

None.

Acknowledgements

This work was supported by the Jiangxi Provincial Natural Science Foundation (20232BAB214067), (20242BAB20221), and the Jiangxi Province Key Laboratory of Advanced Civil Engineering Materials and Green Intelligent Construction (2024SSY05181). We would like to thank anonymous reviewers and the editors of *Energy* for their helpful comments and suggestions.

References

[1] Li H, Zheng J, Zhang Y, Zhang R. Urban morphology and residential building net-zero energy performance: A global meta-analysis. Energy Build 2025;346. https://doi.org/10.1016/j.enbuild.2025.116142.

[2] Yu Y, Cheng J, You S, Ye T, Zhang H, Fan M, et al. Effect of implementing building energy efficiency labeling in China: A case study in Shanghai. Energy Policy 2019;133:1–12. https://doi.org/10.1016/j.enpol.2019.110898.

[3] Guo F, Kurdgelashvili L, Bengtsson M, Akenji L. Analysis of achievable residential energy-saving potential and its implications for effective policy interventions: A study of Xiamen city in southern China. Renewable and Sustainable Energy Reviews 2016;62:507–20. https://doi.org/10.1016/j.rser.2016.04.070.

[4] Ayikoe Tettey UY, Gustavsson L. Energy savings and overheating risk of deep energy renovation of a multi-storey residential building in a cold climate under climate change. Energy 2020;202. https://doi.org/10.1016/j.energy.2020.117578.

[5] Yang X, Zhang S, Xu W. Impact of zero energy buildings on medium-to-long term building energy consumption in China. Energy Policy 2019;129:574–86. https://doi.org/10.1016/j.enpol.2019.02.025.

[6] Liu Z, Liu Y, He BJ, Xu W, Jin G, Zhang X. Application and suitability analysis of the key technologies in nearly zero energy buildings in China. Renewable and Sustainable Energy Reviews 2019;101:329–45. https://doi.org/10.1016/j.rser.2018.11.023.

[7] Zhang D, Ding Y, Wang Y, Fan L. Towards ultra-low energy consumption buildings: Implementation path strategy based on practical effects in China. Energy for Sustainable Development 2022;70:537–48. https://doi.org/10.1016/j.esd.2022.08.025.

[8] Cao X, Yao R, Ding C, Zhou N, Yu W, Yao J, et al. Energy-quota-based integrated solutions for heating and cooling of residential buildings in the Hot Summer and Cold Winter zone in China. Energy Build 2021;236. https://doi.org/10.1016/j.enbuild.2021.110767.

[9] Goudarzi H, Mostafaeipour A. Energy saving evaluation of passive systems for residential buildings in hot and dry regions. Renewable and Sustainable Energy Reviews 2017;68:432–46. https://doi.org/10.1016/j.rser.2016.10.002.

[10] Kheiri F. A review on optimization methods applied in energy-efficient building geometry and envelope design. Renewable and Sustainable Energy Reviews 2018;92:897–920. https://doi.org/10.1016/j.rser.2018.04.080.

[11] Kang Y, Cui Y, Zhang D, Xu W, Pang F, Lu S, et al. Comprehensive photovoltaic system in roofs, opaque walls, and windows toward zero-energy buildings utilizing multi-objective optimization. Journal of Building Engineering 2025;104. https://doi.org/10.1016/j.jobe.2025.112320.

[12] Shi Y, Chen P. Energy retrofitting of hospital buildings considering climate change: An approach integrating automated machine learning with NSGA-III for multi-objective optimization. Energy Build 2024;319. https://doi.org/10.1016/j.enbuild.2024.114571.

[13] Acar U, Kaska O, Tokgoz N. Multi-objective optimization of building envelope components at the preliminary design stage for residential buildings in Turkey. Journal of Building Engineering 2021;42. https://doi.org/10.1016/j.jobe.2021.102499.

[14] Wang R, Lu S, Feng W. A three-stage optimization methodology for envelope design of passive house considering energy demand, thermal comfort and cost. Energy 2020;192.

https://doi.org/10.1016/j.energy.2019.116723.

[15] Kilis V, Ploskas N, Panaras G. Investigation of multi-objective decision making approaches for the optimization in building envelope thermal design. Sustainable Energy Technologies and Assessments 2025;82:104506. https://doi.org/10.1016/j.seta.2025.104506.

[16] Xue Q, Wang Z, Chen Q. Multi-objective optimization of building design for life cycle cost and CO2 emissions: A case study of a low-energy residential building in a severe cold climate. Build Simul 2022;15:83–98. https://doi.org/10.1007/s12273-021-0796-5.

[17] Gou S, Nik VM, Scartezzini J-L, Zhao Q, Li Z. Passive design optimization of newly-built residential buildings in Shanghai for improving indoor thermal comfort while reducing building energy demand. Energy Build 2018;169:484–506. https://doi.org/https://doi.org/10.1016/j.enbuild.2017.09.095.

[18] Fesanghary M, Asadi S, Geem ZW. Design of low-emission and energy-efficient residential buildings using a multi-objective optimization algorithm. Build Environ 2012;49:245–50. https://doi.org/10.1016/j.buildenv.2011.09.030.

[19] Jung Y, Heo Y, Lee H. Multi-objective optimization of the multi-story residential building with passive design strategy in South Korea. Build Environ 2021;203. https://doi.org/10.1016/j.buildenv.2021.108061.

[20] Zhang G, Wu H, Liu J, Huang H, Liu Y. A multi-objective design optimization for the exterior wall coatings of residential buildings in hot summer and warm winter regions. Build Environ 2024;262. https://doi.org/10.1016/j.buildenv.2024.111776.

[21] Li M, Zhao S, Yao S, Huo Q, Yuan J, Li Y. A performance-responsive generative design framework integrating multi-objective optimization for the layout of residential buildings oriented towards low-carbon emission: A case study of Tianjin in China. Journal of Building Engineering 2025;108. https://doi.org/10.1016/j.jobe.2025.112805.

[22] Chen R, Tsay YS, Zhang T. A multi-objective optimization strategy for building carbon emission from the whole life cycle perspective. Energy 2023;262. https://doi.org/10.1016/j.energy.2022.125373.

[23] Wu X, Feng Z, Chen H, Qin Y, Zheng S, Wang L, et al. Intelligent optimization framework of near zero energy consumption building performance based on a hybrid machine learning algorithm. Renewable and Sustainable Energy Reviews 2022;167. https://doi.org/10.1016/j.rser.2022.112703.

[24] Li L, Qi Z, Ma Q, Gao W, Wei X. Evolving multi-objective optimization framework for early-stage building design: Improving energy efficiency, daylighting, view quality, and thermal comfort. Build Simul 2024;17:2097–123. https://doi.org/10.1007/s12273-024-1178-6.

[25] Chen B, Liu Q, Chen H, Wang L, Deng T, Zhang L, et al. Multiobjective optimization of building energy consumption based on BIM-DB and LSSVM-NSGA-II. J Clean Prod 2021;294. https://doi.org/10.1016/j.jclepro.2021.126153.

[26] Chen R, Tsay YS, Ni S. An integrated framework for multi-objective optimization of building performance: Carbon emissions, thermal comfort, and global cost. J Clean Prod 2022;359. https://doi.org/10.1016/j.jclepro.2022.131978.

[27] Xu Y, Zhang G, Yan C, Wang G, Jiang Y, Zhao K. A two-stage multi-objective optimization method for envelope and energy generation systems of primary and secondary school teaching buildings in China. Build Environ 2021;204. https://doi.org/10.1016/j.buildenv.2021.108142.

[28] Yong Z, Li-juan Y, Qian Z, Xiao-yan S. Multi-objective optimization of building energy performance using a particle swarm optimizer with less control parameters. Journal of Building Engineering 2020;32. https://doi.org/10.1016/j.jobe.2020.101505.

[29] Vukadinović A, Radosavljević J, Đorđević A, Protić M, Petrović N. Multi-objective optimization of energy performance for a detached residential building with a sunspace using the NSGA-II genetic algorithm. Solar Energy 2021;224:1426–44. https://doi.org/10.1016/j.solener.2021.06.082.

[30] Ma H, Zhang Y, Sun S, Liu T, Shan Y. A comprehensive survey on NSGA-II for multi-objective optimization and applications. Artif Intell Rev 2023;56:15217–70. https://doi.org/10.1007/s10462-023-10526-z.

[31] Son H, Kim C. Evolutionary many-objective optimization for retrofit planning in public buildings: A comparative study. J Clean Prod 2018;190:403–10. https://doi.org/https://doi.org/10.1016/j.jclepro.2018.04.102.

[32] Cheraghi R, Hossein Jahangir M. Multi-objective optimization of a hybrid renewable energy system supplying a residential building using NSGA-II and MOPSO algorithms. Energy Convers Manag 2023;294:117515. https://doi.org/https://doi.org/10.1016/j.enconman.2023.117515.

[33] Luo Z, Zhu N, Zhao X, Chang J. Whole life cycle energy, economy, and environment collaborative optimization on a building envelope integrated with electricity generator system. Renew Energy 2025;255. https://doi.org/10.1016/j.renene.2025.123832.

[34] Xu W, Wu X, Xiong S, Li T, Liu Y. Optimizing the sustainable performance of public buildings: A hybrid machine learning algorithm. Energy 2025;320. https://doi.org/10.1016/j.energy.2025.135283.

[35] Wang P, Hu J, Chen W. A hybrid machine learning model to optimize thermal comfort and carbon emissions of large-space public buildings. J Clean Prod 2023;400:136538. https://doi.org/https://doi.org/10.1016/j.jclepro.2023.136538.

[36] Wang R, Lu S, Feng W, Zhai X, Li X. Sustainable framework for buildings in cold regions of China considering life cycle cost and environmental impact as well as thermal comfort. Energy Reports 2020;6:3036–50. https://doi.org/10.1016/j.egyr.2020.10.023.

[37] Zhu L, Wang B, Sun Y. Multi-objective optimization for energy consumption, daylighting and thermal comfort performance of rural tourism buildings in north China. Build Environ 2020;176. https://doi.org/10.1016/j.buildenv.2020.106841.

[38] Razmi A, Rahbar M, Bemanian M. PCA-ANN integrated NSGA-III framework for dormitory building design optimization: Energy efficiency, daylight, and thermal comfort. Appl Energy 2022;305. https://doi.org/10.1016/j.apenergy.2021.117828.

[39] Wang Y, Hu L, Hou L, Cai W, Wang L, He Y. Study on energy consumption, thermal comfort and economy of passive buildings based on multi-objective optimization algorithm for existing passive buildings. J Clean Prod 2023;425. https://doi.org/10.1016/j.jclepro.2023.138760.

[40] Zhou Y, Tam VW, Le KN. Developing a multi-objective optimization model for improving building's environmental performance over the whole design process. Build Environ 2023;246. https://doi.org/10.1016/j.buildenv.2023.110996.

[41] Wu C, Pan H, Luo Z, Liu C, Huang H. Multi-objective optimization of residential building energy consumption, daylighting, and thermal comfort based on BO-XGBoost-NSGA-II.

Build Environ 2024;254. https://doi.org/10.1016/j.buildenv.2024.111386.

[42] Duan Z, Wang L, Li B, Yao G. Research on multi-objective energy optimization design for multi-story residential buildings in Suzhou region based on artificial neural networks. Case Studies in Thermal Engineering 2025;73:106721. https://doi.org/10.1016/j.csite.2025.106721.

[43] Xie L, Chen T, Joshi N, Li Z. Climate-responsive retrofitting strategy of elderly housing: Health impacts based on data-driven multi-objective optimization of building envelopes. Build Environ 2025;285. https://doi.org/10.1016/j.buildenv.2025.113554.

[44] Han X, Fang T, Wang Y, Wang Z, Xu J. Multi-objective optimization of passive design parameters for rural residences based on GA-BP-NSGA-II: A case study of cold regions in China. Journal of Building Engineering 2025;112. https://doi.org/10.1016/j.jobe.2025.113624.

[45] Hu S, Jiang Y, Yang X, Pan Y, Rong X, Hao B, et al. Ecological Pathway to Achieve Carbon Neutrality in China's Building Sector. Engineering 2025. https://doi.org/10.1016/j.eng.2025.07.006.

[46] Yu Y, You K, Cai W, Feng W, Li R, Liu Q, et al. City-level building operation and end-use carbon emissions dataset from China for 2015–2020. Sci Data 2024;11. https://doi.org/10.1038/s41597-024-02971-4.

[47] Wang Y, Mauree D, Sun Q, Lin H, Scartezzini JL, Wennersten R. A review of approaches to low-carbon transition of high-rise residential buildings in China. Renewable and Sustainable Energy Reviews 2020;131. https://doi.org/10.1016/j.rser.2020.109990.

[48] Yu W, Li B, Jia H, Zhang M, Wang D. Application of multi-objective genetic algorithm to optimize energy efficiency and thermal comfort in building design. Energy Build 2015;88:135–43. https://doi.org/10.1016/j.enbuild.2014.11.063.

[49] MoHURD. GB 55015-2021 General code for energy efficiency and renewable energy application in buildings. China Architecture & Building Press; 2021.

[50] MoHURD. GB/T 51350-2019 Technical standard for nearly zero energy buildings. China Architecture & Building Press; 2019.

[51] Lin Z, Deng S. A study on the thermal comfort in sleeping environments in the subtropics—Measuring the total insulation values for the bedding systems commonly used in the subtropics. Build Environ 2008;43:905–16. https://doi.org/https://doi.org/10.1016/j.buildenv.2007.01.027.

[52] Evaluation standard for indoor thermal environment in civil buildings. GB/T 50785-2012. China Architecture & Building Press; 2012.

[53] Guo X, Chen X, Yu Y, Wei S, Chen W. A simplified modeling method for studying the thermal performance of buildings with vertical greening systems. J Clean Prod 2024;467:142940. https://doi.org/https://doi.org/10.1016/j.jclepro.2024.142940.

[54] Yu Y, Guo X, Ji J, Li Y, Alaka H, Wei S. Developing a Method for Studying the Impact of Connectors on the Energy Performance of Prefabricated Concrete Buildings. In: Dong L, Ding Y, Liu Y, editors. 9th International Conference on Energy and Environmental Science, Cham: Springer Nature Switzerland; 2025, p. 1234–48.

[55] Lira JS, da Silva EA. A systematic literature review of dynamic life cycle assessment in Buildings: Challenges and guidelines. Journal of Building Engineering 2025;111. https://doi.org/10.1016/j.jobe.2025.113503.

[56] Cai S, Zhang B, Cremaschi L. Review of moisture behavior and thermal performance of polystyrene insulation in building applications. Build Environ 2017;123:50–65. https://doi.org/10.1016/j.buildenv.2017.06.034.

[57] Tao M, Yu Y, Zhang H, Ye T, You S, Zhang M. Research on the optimization design of solar energy-gas-fired boiler systems for decentralized heating. Energies (Basel) 2021;14. https://doi.org/10.3390/en14113195.

[58] Wei T. A review of sensitivity analysis methods in building energy analysis. Renewable and Sustainable Energy Reviews 2013;20:411–9. https://doi.org/10.1016/j.rser.2012.12.014.

[59] Gagnon R, Gosselin L, Decker S. Sensitivity analysis of energy performance and thermal comfort throughout building design process. Energy Build 2018;164:278–94. https://doi.org/10.1016/j.enbuild.2017.12.066.

[60] Akter M, Khalil E, Hasan SMdM, Chowdhury MdKH. Artificial Neural Network (ANN) and Adaptive Neuro-fuzzy Inference System (ANFIS) approaches for predicting thermal conductivity of twill woven cotton fabric. Next Research 2025;2:100698. https://doi.org/10.1016/j.nexres.2025.100698.

[61] Zhao R, Zhu N, Zhao X, Luo Z, Chang J. Multi-objective optimization of a novel photovoltaic-thermoelectric generator system based on hybrid enhanced algorithm. Energy 2025;319. https://doi.org/10.1016/j.energy.2025.135046.

[62] Sundaram A. Combined Heat and Power Economic Emission Dispatch Using Hybrid NSGA II-MOPSO Algorithm Incorporating an Effective Constraint Handling Mechanism. IEEE Access 2020;8:13748–68. https://doi.org/10.1109/ACCESS.2020.2963887.

[63] Zitzler E, Brockhoff D, Thiele L. The hypervolume indicator revisited: On the design of Pareto-compliant indicators via weighted integration. In: Obayashi S, Deb K, Poloni C, Hiroyasu T, Murata T, editors. EVOLUTIONARY MULTI-CRITERION OPTIMIZATION, PROCEEDINGS, vol. 4403, 2007, p. 862+.

[64] Auger A, Bader J, Brockhoff D, Zitzler E. Theory of the Hypervolume Indicator: Optimal μ-Distributions and the Choice of the Reference Point. FOGA'09: PROCEEDINGS OF THE 10TH ACM SIGRVO CONFERENCE ON FOUNDATIONS OF GENETIC ALGORITHMS, 2009, p. 87–102.

[65] Sun Y, Yen GG, Yi Z. IGD Indicator-Based Evolutionary Algorithm for Many-Objective Optimization Problems. IEEE Transactions on Evolutionary Computation 2019;23:173–87. https://doi.org/10.1109/TEVC.2018.2791283.

[66] Zapotecas Martinez S, Coello Coello CA. A multi-objective particle swarm optimizer based on decomposition. Proceedings of the 13th Annual Conference on Genetic and Evolutionary Computation, New York, NY, USA: Association for Computing Machinery; 2011, p. 69–76. https://doi.org/10.1145/2001576.2001587.